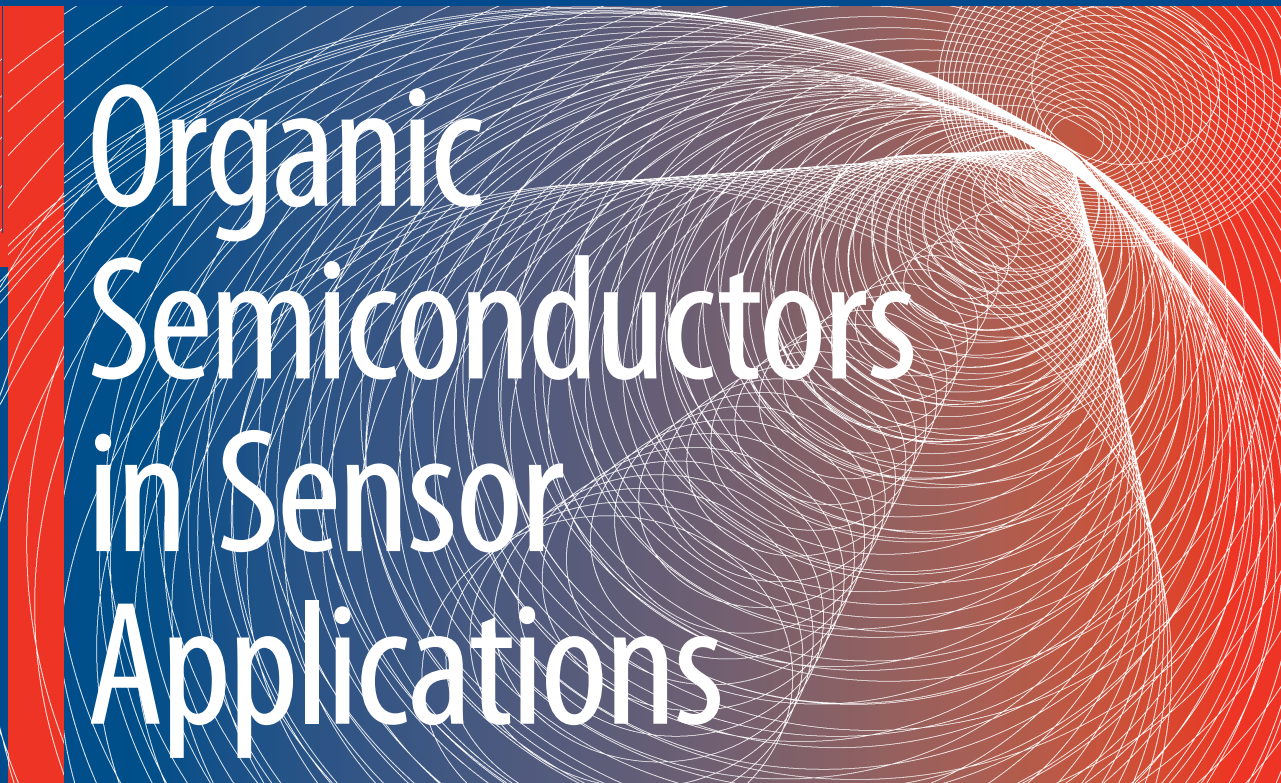


Daniel A. Bernards
Róisín M. Owens
George G. Malliaras
Editors

SPRINGER SERIES IN MATERIALS SCIENCE 107



Organic
Semiconductors
in Sensor
Applications

 Springer

Springer Series in
MATERIALS SCIENCE

Editors: R. Hull R. M. Osgood, Jr. J. Parisi H. Warlimont

The Springer Series in Materials Science covers the complete spectrum of materials physics, including fundamental principles, physical properties, materials theory and design. Recognizing the increasing importance of materials science in future device technologies, the book titles in this series reflect the state-of-the-art in understanding and controlling the structure and properties of all important classes of materials.

- | | | | |
|-----|---|-----|--|
| 99 | Self-Organized Morphology in Nanostructured Materials
Editors: K. Al-Shamery and J. Parisi | 105 | Dilute III-V Nitride Semiconductors and Material Systems
Physics and Technology
Editor: A. Erol |
| 100 | Self Healing Materials
An Alternative Approach to 20 Centuries of Materials Science
Editor: S. van der Zwaag | 106 | Into The Nano Era
Moore's Law Beyond Planar Silicon CMOS
Editor: H.R. Huff |
| 101 | New Organic Nanostructures for Next Generation Devices
Editors: K. Al-Shamery, H.-G. Rubahn, and H. Sitter | 107 | Organic Semiconductors in Sensor Applications
Editors: D.A. Bernards, R.M. Owens, and G.G. Malliaras |
| 102 | Photonic Crystal Fibers
Properties and Applications
By F. Poli, A. Cucinotta, and S. Selleri | 108 | Evolution of Thin-Film Morphology
Modeling and Simulations
By M. Pelliccione and T.-M. Lu |
| 103 | Polarons in Advanced Materials
Editor: A.S. Alexandrov | 109 | Reactive Sputter Deposition
Editors: D. Depla and S. Mahieu |
| 104 | Transparent Conductive Zinc Oxide
Basics and Applications in Thin Film Solar Cells
Editors: K. Ellmer, A. Klein, and B. Rech | 110 | The Physics of Organic Superconductors and Conductors
Editor: A.G. Lebed |

Volumes 50–98 are listed at the end of the book.

D.A. Bernards R.M. Owens
G.G. Malliaras
Editors

With 183 Figures

Dr. Daniel A. Bernardis
Professor George G. Malliaras
Cornell University, Department of Materials Science and Engineering
327 Bard Hall, Ithaca, NY 14853, USA
E-mail: dab68@cornell.edu, ggm1@cornell.edu

Dr. Róisín M. Owens
Cornell University, Department of Biomedical Engineering
The Baker Institute, Hungerford Hill Road, Ithaca, NY 14853, USA
E-mail: ro27@cornell.edu

Series Editors:

Professor Robert Hull
University of Virginia
Dept. of Materials Science and Engineering
Thornton Hall
Charlottesville, VA 22903-2442, USA

Professor Jürgen Parisi
Universität Oldenburg, Fachbereich Physik
Abt. Energie- und Halbleiterforschung
Carl-von-Ossietzky-Strasse 9-11
26129 Oldenburg, Germany

Professor R. M. Osgood, Jr.
Microelectronics Science Laboratory
Department of Electrical Engineering
Columbia University
Seeley W. Mudd Building
New York, NY 10027, USA

Professor Hans Warlimont
Institut für Festkörper-
und Werkstofforschung,
Helmholtzstrasse 20
01069 Dresden, Germany

ISSN 0933-033X

ISBN 978-3-540-76313-0 Springer Berlin Heidelberg New York

Library of Congress Control Number: 2007938413

All rights reserved.

No part of this book may be reproduced in any form, by photostat, microfilm, retrieval system, or any other means, without the written permission of Kodansha Ltd. (except in the case of brief quotation for criticism or review.)

This work is subject to copyright. All rights are reserved, whether the whole or part of the material is concerned, specifically the rights of translation, reprinting, reuse of illustrations, recitation, broadcasting, reproduction on microfilm or in any other way, and storage in data banks. Duplication of this publication or parts thereof is permitted only under the provisions of the German Copyright Law of September 9, 1965, in its current version, and permission for use must always be obtained from Springer. Violations are liable to prosecution under the German Copyright Law.

Springer is a part of Springer Science+Business Media.
springer.com

© Springer-Verlag Berlin Heidelberg 2008

The use of general descriptive names, registered names, trademarks, etc. in this publication does not imply, even in the absence of a specific statement, that such names are exempt from the relevant protective laws and regulations and therefore free for general use.

Typesetting: Data prepared by SPi using a Springer L^AT_EX macro package
Cover concept: eStudio Calamar Steinen
Cover production: WMX Design GmbH, Heidelberg

Printed on acid-free paper SPIN: 12037421 57/3180/SPi 5 4 3 2 1 0

Preface

One of the most exciting developments of the past two decades has been the emergence of organic electronics. This term refers to the use of organic materials as active layers in a variety of semiconductor devices. One example is organic light emitting diodes, devices which emit visible light upon the passage of current through an organic semiconductor film. These devices are now commercially available in small format flat panel displays and are being intensely developed for solid-state lighting. A second example is organic thin film transistors, which control the flow of electricity in circuits and are being developed for applications in smart tags and flat panel displays.

Concurrently, our need for sensors is ever increasing. Food safety, environmental monitoring, medical diagnostics, and homeland security are all areas that would benefit from the deployment of sensors and sensor networks. Improvements would be useful or even required on multiple fronts, including sensitivity and specificity, power consumption, portability, and cost. Organic semiconductors offer many advantages in comparison with their inorganic counterparts, which make them particularly attractive for sensor applications. First, they can be deposited at or near room temperature on large area surfaces and are compatible with mechanically flexible supports such as paper and plastic. This enables their use in roll-to-roll fabrication techniques, which can dramatically decrease manufacturing costs, an important attribute for disposable sensors. Second, their properties can be tailored by means of chemical synthesis. This includes electronic properties (such as energy gap and electron affinity) but also properties such as surface energy. Of particular interest for sensors is the ability to covalently attach biologically relevant moieties to organic semiconductor molecules. Such hybrid materials have the potential to lead to the fabrication of sensors with high sensitivity and specificity.

It is important to note that the main drawbacks of organic semiconductor devices are not detrimental to their application in sensors: Low-end performance, for example in terms of device speed, prohibits organics semiconductor devices from competing with silicon in high-end computing applications. This does not, however, constitute a limitation, as sensors can tolerate considerably

slower detection speeds. Moreover, long-term stability issues, which often plague organic semiconductor devices, are not relevant for disposable sensors. Therefore, sensors represent an application that can benefit from all the advantages of organic semiconductors and in principle suffers from none of the limitations. Quite naturally, the application of organic semiconductors and their devices in sensors has been attracting increased attention in the past few years.

This book covers central research directions in this rapidly emerging field. The first two chapters discuss fluorescence-based sensors and show how one can tailor organic semiconductors to yield large changes in their emission properties upon interaction with an analyte. The next two chapters deal with the application of organic light emitting diodes and photodetectors in sensors and their integration with lab-on-a-chip concepts. A variety of solid state devices are analyzed in the fifth chapter and the applications of lasing and photoconducting organic devices in sensors are proposed. The emphasis then shifts to electrical detection, first with field-effect transistors and then with electrochemical ones. In the remaining four chapters the mechanism of operation, the merits, and the potential applications of these devices in signal transduction are discussed.

We believe that the application of organic semiconductors and their devices in sensors will experience significant growth in the years to come. We hope that this book will serve as a useful text and reference for this emerging field.

Ithaca, New York, 2007

Dan Bernards
Róisín Owens
George Malliaras

Contents

1 Water Soluble Poly(fluorene) Homopolymers and Copolymers for Chemical and Biological Sensors

<i>G.C. Bazan and S. Wang</i>	1
1.1 Introduction	1
1.2 General Structures and Properties	2
1.2.1 Design, Synthesis, and Structural Properties	2
1.2.2 Optical Properties	6
1.3 Signal Transduction Mechanisms in Sensors	9
1.4 Chemo- and Biosensor Applications	15
1.4.1 DNA Sensors	15
1.4.2 RNA Sensors	23
1.4.3 Protein Detection	25
1.4.4 Glucose Sensors	28
1.4.5 Detection of Other Small Molecules	30
1.5 Heterogeneous Platforms	31
1.6 Summary and Outlook	32
References	34

2 Polyelectrolyte-Based Fluorescent Sensors

<i>K. Ogawa, K.E. Achyuthan, S. Chemburu, E. Ji, Y. Liu, G.P. Lopez, K.S. Schanze, and D.G. Whitten</i>	39
2.1 General Introduction	39
2.1.1 Amplified Fluorescence Quenching	39
2.1.2 General Sensor Schemes: Bioassays Based on Quench/Unquench	43
2.2 Enzyme Activity Assays	44
2.2.1 Assay Formats and Types	44
2.2.2 Proteolytic Enzyme Assays Using Conjugated Polyelectrolytes	45
2.2.3 Phospholipase Assays Using Conjugated Polyelectrolytes	46
2.2.4 Assays Based on “Frustrated Super-Quenching”	49

2.2.5 Supramolecular Self-Assembly and Scaffold Disruption/Destruction Assays	50
2.2.6 Cyanines and Supra-Molecular Self-Assembly	50
2.2.7 Cyanine Chemistry	51
2.2.8 Glycosidases and Scaffold Disruption/Destruction Assay	52
2.3 Conjugated Polyelectrolyte Surface-Grafted Colloids	54
2.4 Summary and Conclusions	57
References	58

3 Structurally Integrated Photoluminescent Chemical and Biological Sensors: An Organic Light-Emitting Diode-Based Platform

<i>R. Shinar and J. Shinar</i>	61
3.1 Introduction	61
3.1.1 Photoluminescence-Based Sensors	61
3.1.2 Structurally Integrated OLED/Sensing Component Modules	62
3.1.3 Structural Integration of the OLED Array/Sensing Film	63
3.2 Single Analyte Monitoring	64
3.2.1 Gas-Phase and Dissolved Oxygen	64
3.2.2 Enhanced Photoluminescence of Oxygen-Sensing Films Through Doping with Titania Particles [70]	69
3.2.3 Glucose	71
3.2.4 Hydrazine (N ₂ H ₄)	77
3.2.5 Anthrax Lethal Factor (LF)	79
3.3 Advanced Sensor Arrays	81
3.3.1 OLED-Based Multiple Analyte Sensing Platform	81
3.3.2 Extended Structural Integration: OLED/Sensing Component/Photodetector Integration	87
3.4 Future Directions	90
3.4.1 Improved OLEDs	90
3.4.2 Sensor Microarrays	91
3.4.3 Autonomous Field-Deployable Sensors for Biological Agents	91
3.5 Summary and Concluding Remarks	92
References	92

4 Lab-on-a-Chip Devices with Organic Semiconductor-Based Optical Detection

<i>O. Hofmann, D.D.C. Bradley, J.C. deMello, and A.J. deMello</i>	97
4.1 Introduction	97
4.1.1 Microfluidics and Lab-on-a-Chip	97
4.1.2 Detection Problem at the Microscale	102
4.2 Fabrication	103
4.2.1 Microfluidic Systems	103

4.2.2 Organic Semiconductor-Based Light Sources and Detectors	108
4.2.3 Towards Mass Manufacture	112
4.3 Functional Optical Components	116
4.3.1 OLED Light Sources for Microchip Analysis	116
4.3.2 Organic Photodetectors for Chemiluminescence Assays	118
4.3.3 Optical Filters for Head-On Fluorescence Detection	123
4.4 Applications	126
4.4.1 Microalbuminuria Determination On-Chip	127
4.4.2 Chemiluminescence-Based Diagnostic Tests	131
4.4.3 Towards Portable and Disposable Diagnostic Devices	135
4.5 Conclusions and Outlook	137
References	139
5 Solid-State Chemosensitive Organic Devices for Vapor-Phase Detection	
<i>J. Ho, A. Rose, T. Swager, and V. Bulović</i>	141
5.1 Introduction	141
5.1.1 Chemical Sensors and Electronic Noses	141
5.2 Survey of State-of-the-Art Vapor-Phase Solid-State Chemosensing Organic Devices	142
5.2.1 Electrical Odor Sensors	144
5.2.2 Optical Odor Sensor	152
5.2.3 Summary	160
5.3 Recent Advances	160
5.3.1 Chemosensing Lasing Action	160
5.3.2 Chemical Sensing Heterojunction Photoconductors	172
References	180
6 Detection of Chemical and Physical Parameters by Means of Organic Field-Effect Transistors	
<i>A. Bonfiglio, I. Manunza, P. Cosseddu, and E. Orgiu</i>	185
6.1 Introduction	185
6.2 An Overview of Organic Field-Effect Sensors	186
6.3 (Bio)chemosensing in Solution	188
6.3.1 Ion Sensitive Organic Field-Effect Transistors (ISOFETs)	188
6.4 Strain and Pressure Sensors	193
6.4.1 State of the Art of Mechanical Sensors Including OFETs	194
6.4.2 Flexible Structures for Mechanical Sensors	199
6.5 Design and Technology of Organic Field-Effect Sensors	202
6.6 Applications for Organic Field-Effect Sensors	205
6.6.1 Artificial Sense of Touch	206
6.6.2 E-Textiles	208
6.7 Conclusions	210
References	210

7 Performance Requirements and Mechanistic Analysis of Organic Transistor-Based Phosphonate Gas Sensors	
<i>K. See, J. Huang, A. Becknell, and H. Katz</i>	213
7.1 Overview of Electronic Sensors for Chemical Vapors and Warfare Agents	213
7.1.1 Introduction and Response Targets	213
7.1.2 Selectivity	214
7.1.3 Stability	215
7.1.4 Response Time	216
7.1.5 Power Consumption and Form Factor	216
7.2 Organic Semiconductor Transistor Sensors	216
7.2.1 Organic Electronics and Chemical Sensing	216
7.2.2 Electronic Transduction Mechanism	218
7.3 Testing Environments for Prototype Sensing Elements	219
7.3.1 Test Chambers	219
7.3.2 Device Packaging	225
7.4 Electrical Test Procedures	225
7.4.1 Generation of Saturation Curves at a Fixed Time Interval	225
7.4.2 Generation of Transfer Curves at a Fixed Time Interval	226
7.4.3 Pulsed Vs. Nonpulsed Measurements	227
7.4.4 Erasing Electrical History	227
7.5 Responses of Functionalized Organic Semiconductors to DMMP	228
7.5.1 Responses of Functionalized Hole-Transporting Oligomers, Including Blends and Surface Modifications	229
7.5.2 Responses of Electron-Transporting Films, Including Hydroxylated Island Overlayers	232
7.6 Data Analysis	234
7.6.1 Sensitivity of an OFET Sensor: Gate Voltage Dependence and Contributions of Mobility and Threshold Voltage Changes	234
7.6.2 Self-Consistent Equation Based on Simple Saturation Current	235
7.6.3 Contributions of Gate Dependent Mobility and Contact Resistance	238
7.7 Sensing Mechanisms and OFET Models	239
7.8 Summary and Outlook	242
References	243
8 Electrochemical Transistors for Applications in Chemical and Biological Sensing	
<i>A. Kumar and J. Sinha</i>	245
8.1 Introduction	245
8.2 Sensors Based on Electrochemical Transistors	247
8.2.1 Sensor Mechanisms	248
8.2.2 Enzyme-Based Sensing	251

8.2.3 Antibody–Antigen-Based Sensing	255
8.2.4 DNA-Based Sensing	257
8.3 Recent advances in Design and Fabrication of Electrochemical Transistors	258
8.4 Summary and Future Directions	260
References	261
9 PEDOT:PSS-Based Electrochemical Transistors for Ion-to-Electron Transduction and Sensor Signal Amplification	
<i>M. Berggren, R. Forchheimer, J. Bobacka, P.-O. Svensson, D. Nilsson, O. Larsson, and A. Ivaska</i>	<i>263</i>
9.1 The PEDOT:PSS-Based Electrochemical Organic Thin Film Transistor	263
9.1.1 Electrochemical Transistors: A Brief Introduction and a Short Historical Review	263
9.1.2 The Operation Principle of the PEDOT:PSS-Based Electrochemical Organic Thin Film Transistor	264
9.1.3 Design Criteria and Device Operation Parameters	265
9.1.4 Manufacturing Techniques	267
9.2 The PEDOT:PSS OECT as an Ion-to-Electron Transducer	269
9.2.1 Different Sensor Principles of the PEDOT:PSS Electrochemical Transistor	269
9.2.2 Humidity Sensing	269
9.2.3 Ion-Selective Membranes	270
9.3 The PEDOT:PSS Electrochemical transistor in logic and amplification circuits	272
9.3.1 Introduction to Electrochemical Circuits and Systems	272
9.3.2 Electrochemical Digital Circuits	273
9.3.3 Electrochemical Analog Circuits	273
9.3.4 The Differential Amplifier	276
9.3.5 Zero Detector	277
9.3.6 Oscillators	277
9.4 Outlook	278
References	279
Index	281

Contributors

K.E. Achyuthan

Department of Biosensors and
Nanomaterials, Sandia National
Laboratories
Albuquerque, NM 87123, USA

G.C. Bazan

Departments of Materials
and Chemistry & Biochemistry,
University of California
Santa Barbara, CA 93106, USA

A. Becknell

Applied Physics Laboratory,
Johns Hopkins University
Laurel, MD 20723, USA

M. Berggren

Organic Electronics, ITN,
Linköpings Universitet
SE-601 74 Norrköping, Sweden

J. Bobacka

Laboratory of Analytical Chemistry,
Process Chemistry Centre,
Åbo Akademi
Biskopsgatan 8
FI-20500 Åbo-Turku, Finland

A. Bonfiglio

Department of Electrical
and Electronic Engineering,
University of Cagliari,
and INFM-CNR S3 Centre
Modena, Italy

D.D.C. Bradley

Department of Physics,
Imperial College London
South Kensington
London SW7 2AZ, UK

V. Bulović

Department of Electrical Engineering
and Computer Science,
Massachusetts Institute
of Technology
Cambridge, MA 02139, USA

S. Chemburu

Department of Chemical and Nuclear
Engineering,
Center for Biomedical Engineering,
University of New Mexico
Albuquerque, NM 87131, USA

P. Cosseddu

Department of Electrical
and Electronic Engineering,
University of Cagliari,
and INFM-CNR S3 Centre
Modena, Italy

XIV Contributors

A.J. deMello

Department of Chemistry
Imperial College London
South Kensington
London SW7 2AZ, UK

J.C. deMello

Department of Chemistry
Imperial College London
South Kensington
London SW7 2AZ, UK

R. Forchheimer

Image Coding, ISY
Linköpings Universitet
SE-581 83 Linköping, Sweden

J. Ho

Department of Electrical Engineering
and Computer Science,
Massachusetts Institute
of Technology
Cambridge, MA 02139, USA

O. Hofmann

Molecular Vision Ltd, BioIncubator
Unit, Bessemer Building (RSM)
Level 1, Prince Consort Road
London SW7 2BP, UK

J. Huang

Department of Materials Science
and Engineering
Johns Hopkins University
Baltimore, MD 21218, USA

A. Ivaska

Laboratory of Analytical Chemistry,
Process Chemistry Centre,
Åbo Akademi
Biskopsgatan 8
FI-20500 Åbo-Turku, Finland

E. Ji

Department of Chemistry,
University of Florida
Gainesville, FL 32611, USA

H. Katz

Department of Materials Science
and Engineering
Johns Hopkins University,
Baltimore, MD 21218, USA

A. Kumar

Department of Chemistry, Indian
Institute of Technology Bombay
Mumbai 400076, India

O. Larsson

Organic Electronics, ITN,
Linköpings Universitet
SE-601 74 Norrköping, Sweden

Y. Liu

Department of Chemistry,
University of Florida
Gainesville, FL 32611, USA

G.P. Lopez

Department of Chemical
and Nuclear Engineering,
Center for Biomedical Engineering,
University of New Mexico
Albuquerque, NM 87131, USA

I. Manunza

Department of Electrical
and Electronic Engineering,
University of Cagliari,
and INFN-CNR S3 Centre
Modena, Italy

D. Nilsson

Acreo AB, Bredgatan 34
SE-602 21 Norrköping, Sweden

K. Ogawa

Department of Chemistry,
University of Florida
Gainesville, FL 32611, USA

E. Orgiu

Department of Electrical
and Electronic Engineering,
University of Cagliari,
and INFM-CNR S3 Centre
Modena, Italy

A. Rose

Department of Chemistry,
Massachusetts Institute of
Technology
Cambridge, MA 02139, USA

K.S. Schanze

Department of Chemistry,
University of Florida
Gainesville, FL 32611, USA

K. See

Department of Materials Science
and Engineering,
Johns Hopkins University
Baltimore, MD 21218, USA

J. Shinar

Ames Laboratory-USDOE
and Department of Physics and
Astronomy, Iowa State University
Ames, IA 50011, USA

R. Shinar

Microelectronics Research Center,
Iowa State University
Ames, IA 50011, USA

J. Sinha

Department of Chemistry, Indian
Institute of Technology Bombay
Mumbai 400076, India

P.-O. Svensson

Organic Electronics, ITN,
Linköpings Universitet
SE-601 74 Norrköping, Sweden

T. Swager

Department of Chemistry,
Massachusetts Institute of
Technology
Cambridge, MA 02139, USA

S. Wang

Key Laboratory of Organic Solids,
Institute of Chemistry,
Chinese Academy of Sciences
Beijing 100080, P.R. China

D.G. Whitten

Department of Chemical
and Nuclear Engineering,
Center for Biomedical Engineering,
University of New Mexico
Albuquerque, NM 87131, USA

Water Soluble Poly(fluorene) Homopolymers and Copolymers for Chemical and Biological Sensors

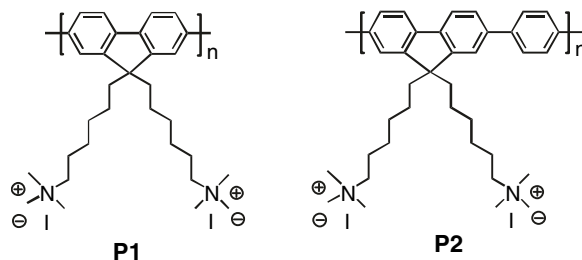
G.C. Bazan and S. Wang

1.1 Introduction

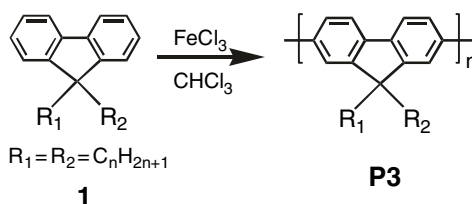
Conjugated polymers (CPs) are characterized by a delocalized electronic structure. These materials have established themselves as useful components in optoelectronic devices such as light-emitting diodes (LEDs), field effect transistors (FETs), and photovoltaic devices [1–3]. Less explored is their use in chemical or biological sensor applications, particularly in homogeneous formats. The chemical structures of CPs offer several advantages as the responsive element in optical, chemical, and biological-detection schemes. As a result of their electronic structure, one often observes very efficient coupling between optoelectronic segments [4–14]. Excitations can be efficiently transferred to lower energy electron/energy acceptor sites over long distances in ways not easily accessible for assemblies of weakly interacting chromophores. Charge transport [15], conductivity [16–19], emission efficiency [20], and exciton migration [2] are easily perturbed by external agents, leading to large changes in measurable signals [21]. Trace detection of analytes has been successfully accomplished by making use of these amplification mechanisms [22–40].

Solubility in aqueous media is essential for interfacing with biological analytes. Water-soluble conjugated polymers typically incorporate charged functionalities as pendant groups on the conjugated backbone [41]. This class of materials, often referred to as conjugated polyelectrolytes, embody the semiconducting and optical properties of conjugated polymers and the complex charge-mediated behavior of polyelectrolytes. From the perspective of developing biosensors, the charged nature of the polymers provides for a convenient tool to control the average distance between optical partners. A widely used approach involves coordinating electrostatic interactions upon target recognition by a probe structure.

Of the various primary conjugated polymer backbones, such as poly(*p*-phenylenevinylene)s, poly(thiophene)s, poly(phenyleneethynylene), etc., [42] poly(fluorene) and related structures have been widely used in biological



Scheme 1.1. Molecular structures of a water-soluble poly(fluorene) (**P1**) and a poly(fluorene-*alt*-phenylene) (**P2**)



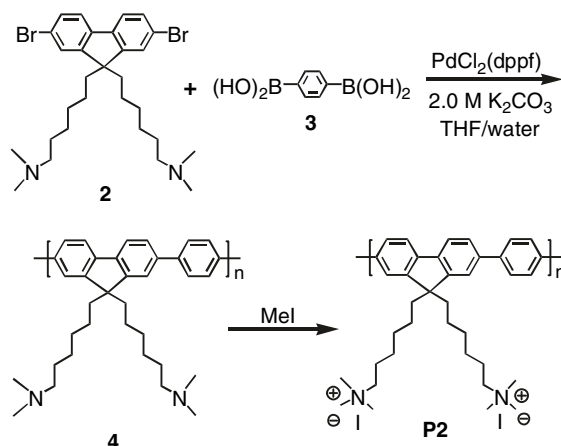
Scheme 1.2. The synthetic scheme of the soluble poly(fluorene) **P3**

and chemical sensing applications because of their facile substitution at the fluorene C9 position, good chemical and thermal stability, and high fluorescence quantum yields in water [43]. Typical molecular structures include the homopolymer **P1** and the copolymer **P2**, which are shown in Scheme 1.1. The purpose of this review is to highlight some of the fundamental properties of charged poly(fluorene)s and related copolymers and their use in optical sensory processes. Preparation methods are provided, which serve to emphasize typical synthetic approaches but do not constitute an exhaustive list of published procedures. The function and properties of conjugated polyelectrolytes with repeat units other than fluorene can be found in the literature [20–40].

1.2 General Structures and Properties

1.2.1 Design, Synthesis, and Structural Properties

The first synthesis of a soluble and processible poly(2,7-fluorene) was reported by Yoshino and coworkers in 1989 [44, 45]. Their approach involved coupling fluorene monomers with substituents at the C9 position by chemical oxidation with FeCl₃ (see **P3** in Scheme 1.2). However, the polymerization process was not regiospecific and the polymer backbone contained structural defects that influence the electronic delocalization. Thus, the synthesis of defect-free poly(fluorene)s became a major challenge and advances in carbon–carbon bond forming reactions promoted by organometallic catalysts provided the

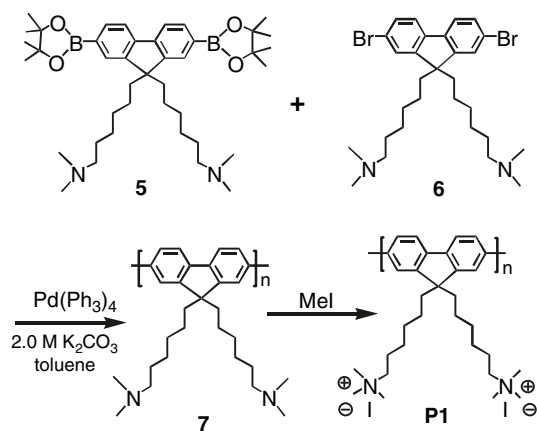


Scheme 1.3. The synthetic scheme of the water-soluble copolymer **P2**

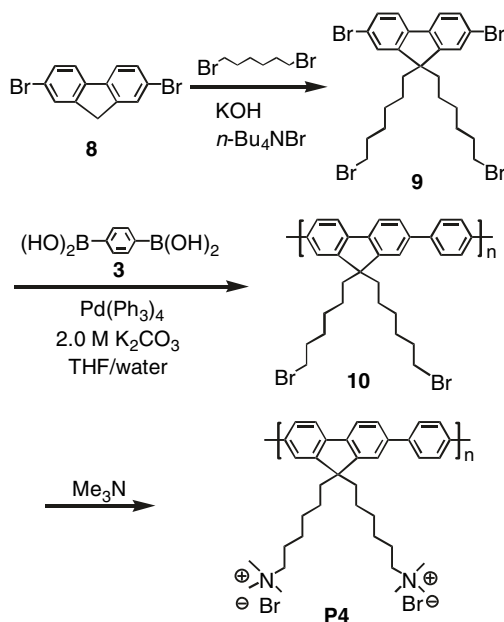
solution. The most popular polymerization methods include Suzuki, Stille, and Yamamoto coupling reactions [46, 47].

Water-soluble copolymers containing fluorene repeat units were initially prepared by quaternization with methyl iodide of pendant amine groups on a neutral precursor, as shown in Scheme 1.3 [48]. Neutral precursor materials are particularly useful for proper characterization because of their solubility in common organic solvents. Special care must be taken during the “charging up” of the polymer structure by way of reactions such as quaternization reactions (cationic backbones) or deprotonation steps (anionic backbones). These reactions transform a material that is soluble in nonpolar solvents into one that is soluble in polar media. Precipitation can take place during the transition, which limits the degree of quaternization and the final solubility in water. To circumvent this problem, the solvent is changed during the course of the reaction to avoid formation of polymer particles or deposition of the product onto the reaction vessel surface. In the case of Scheme 1.3, the reaction begins in THF and water is added after a few minutes to redissolve the mixture. Purification of the final products is typically accomplished by precipitating into a poor solvent.

The water-soluble homopolymer **P1** was reported via the set of reactions shown in Scheme 1.4 [49]. Quaternization of neutral polymer precursor **7** with methyl iodide in THF/DMF/water gave the desired **P1** target. Because of the difficulty in purifying the monomers containing amine groups, and their propensity to strongly adsorb onto chromatographic supports, an improved synthetic approach was developed, as shown in Scheme 1.5 [15]. In Scheme 1.5, the monomers and the neutral polymer precursor are obtained with high purity. Subsequent quaternization proceeds with excellent yield via the reaction of the precursor polymer **10** with trimethylamine in THF/water, followed by precipitation from acetone.

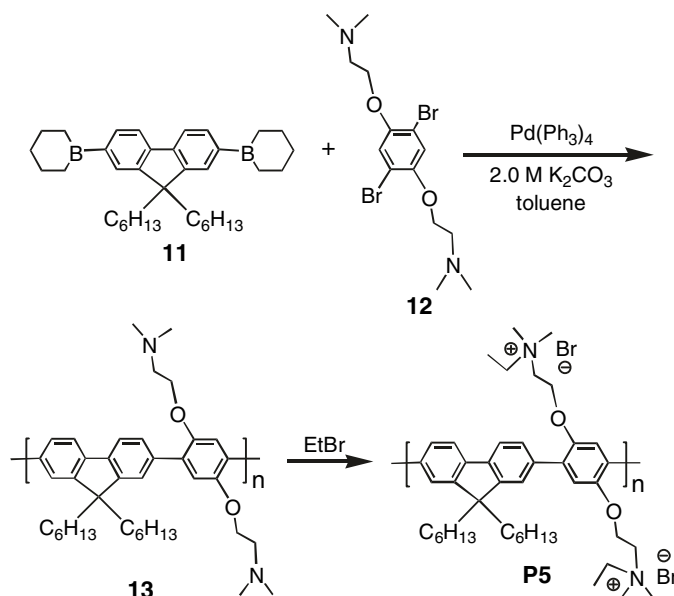


Scheme 1.4. Synthetic entry to the water-soluble poly(fluorene) **P1**

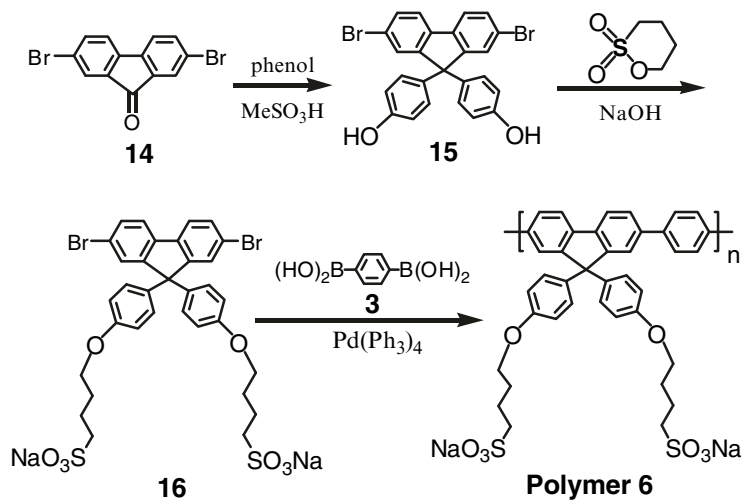


Scheme 1.5. Improved synthetic scheme for the synthesis of the water-soluble copolymer **P4**

The cationic species **P5** in Scheme 1.6 bears charged groups on the phenylene repeat units and was prepared by applying the neutral polymer precursor approach [50]. Specifically, the neutral polymer precursor **13** was obtained by the Suzuki copolymerization using **11** and **12**. Addition of EtBr to **13** provides



Scheme 1.6. The synthesis of the water-soluble cationic poly(fluorene) **P5**



Scheme 1.7. The synthesis of the water-soluble anionic poly(fluorene) **P6**

the target material, which is soluble in DMSO, methanol, and water, and displays negligible solubility in less polar solvents such as THF and CHCl_3 .

The synthesis of the anionic **P6** is shown in Scheme 1.7. Copolymerization of 2,7-dibromo-9,9-bis(4-sulfonylbutoxyphenyl)fluorene (**16**) with 1,4-phenylenediboric acid (**3**) using $\text{Pd(PPh}_3)_4$ produces a polymer that is

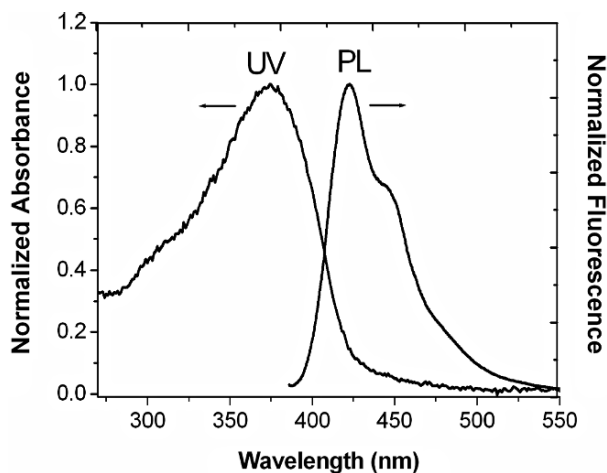


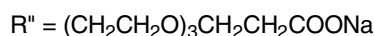
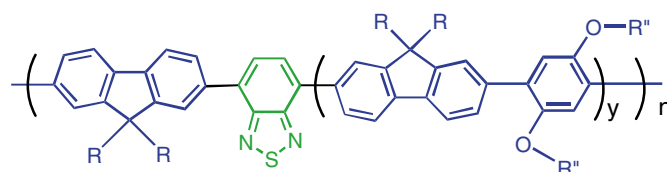
Fig. 1.1. Absorption and PL spectra of **P1** in aqueous solution. The excitation wavelength for PL spectra is 380 nm

soluble in DMSO, methanol, and water [51]. The polymer had a molecular weight of 0.65 kDa, as determined by gel permeation chromatography (GPC).

1.2.2 Optical Properties

Aqueous solutions of charged poly(fluorene)s and their derivatives typically display unstructured absorption spectra with maxima centered at approximately 380 nm. Their photoluminescence (PL) spectra exhibit vibronically well-resolved bands with maxima centered at 420 nm (Fig. 1.1). PL quantum efficiencies in aqueous media are in the range of 20–40%, depending on factors such as the substitution pattern, the degree of aggregation, the nature of counter ions, and ionic content of the medium [48,49,52]. Aggregation in water is a common feature of conjugated polyelectrolytes. This process is driven by the highly hydrophobic backbone and leads to proximity of the optically active units. Increased interchain contact often, but not always, translates to self-quenching and increased rates of energy transfer and photo-induced charge transfer. The number of charges per repeat unit and the nature of the linkers between the backbone and the charged groups influence solubility and thus aggregation tendency. Less soluble polymers exhibit a greater tendency to aggregate [53,54].

A recent study on polymer **P1-BT_x** provides insight into the effect of polymer charge on optical performance and aggregation in aqueous media [55]. The molecular structure of **P1-BT_x** is given in Scheme 1.8. The main backbone is composed of alternating substituted fluorene and phenylene units together with a fractional substitution of the phenylene fragments with 2,1,3-benzothiadiazole (BT) chromophores. The subscript “x” refers to the



P1-BT_x

$$x = \% \text{ BT} = 100/(y+1)$$

Scheme 1.8. Molecular structure of **P1-BT_x**. Reprinted with permission from [55]. Copyright 2006 American Chemical Society

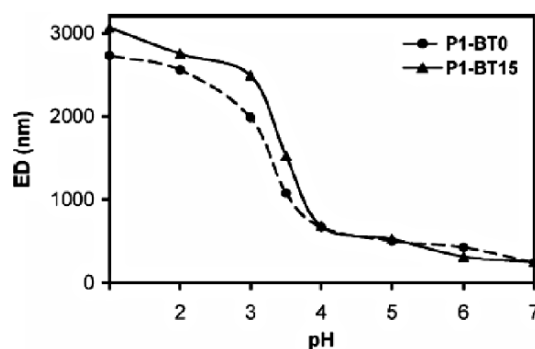


Fig. 1.2. Effective diameter (ED) determined by dynamic light scattering of **P1-BT₀** and **P1-BT₁₅** ($[\text{RU}] = 3.8 \times 10^{-5} \text{ M}$) in water as a function of pH. Reprinted with permission from [55]. Copyright 2006 American Chemical Society

percentage of BT sites relative to the phenylene units. Two specific examples were used in these studies, namely **P1-BT₀** (i.e., no BT units) and **P1-BT₁₅**. Because of the high content of ethylene oxide groups in the backbone substituents, both neutral and anionic versions of the polymer are water-soluble.

Protonation of the carboxylic sites at low pH renders the **P1-BT_x** structures neutral and leads to a decrease in the electrostatic repulsion between chains. Dynamic light scattering analysis (DLS), shown in Fig. 1.2, reveals that both **P1-BT₀** and **P1-BT₁₅** show a sudden increase in particle size when the solution pH is lower than ~ 3.5 . The concentrations of the polymers throughout this chapter are given in terms of repeat units (RUs). These data are in good agreement with substantial interchain aggregation upon protonation of the pendant carboxylic groups. The data in Fig. 1.2 should be interpreted with care since the effective diameters (EDs) are larger than would be anticipated on the basis of single chain molecular dimensions. Several assumptions are made in the treatment of DLS data. Discrepancies between calculated and

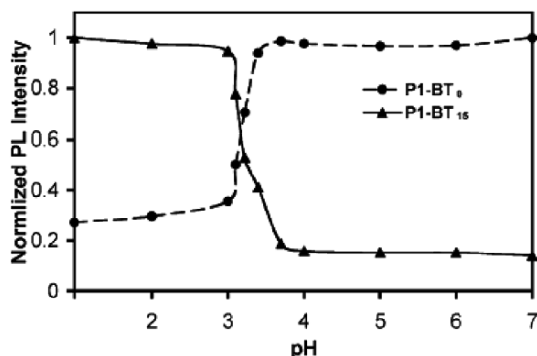
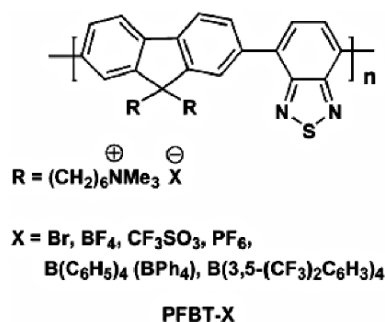


Fig. 1.3. PL response of **P1-BT₀** ($[RU] = 3.8 \times 10^{-5}$ M) and **P1-BT₁₅** ($[RU] = 4.3 \times 10^{-5}$ M) as a function of pH. Data were normalized relative to the maximum PL intensity of each polymer. Reprinted with permission from [55]. Copyright 2006 American Chemical Society

actual values may arise from nonspherical aggregate shapes and from the stiff, rod-like, aspect ratio of the individual chains. Nonetheless, there is a transition to higher aggregates after the pH of the solution becomes acidic enough to neutralize the polymer charge.

Several significant observations were made in the two regimes of Fig. 1.3. Upon aggregation, the PL quantum yield of **P1-BT₀** decreases, possibly as a result of self-quenching via interchain contacts. For **P1-BT₁₅** one observes a change in the emission spectra, from blue to green, as a result of increased fluorescence resonance energy transfer (FRET) from the blue-emitting phenylene-fluorene segments to the BT sites. Additionally, the PL efficiency of the BT chromophores at low pH is considerably higher relative to conditions at high pH. Water induces quenching in the BT emission and aggregation appears to reduce BT/water contacts, ultimately decreasing energy wasting nonradiative relaxation processes, and thereby increasing optical output. Changes in optical properties are reversible when the solution pH is cycled between low and high conditions. Furthermore, as shown in Fig. 1.3, these changes occur at approximately the same pH at which aggregation was detected by DLS experiments. The collective set of observations provides insight into how interchain contacts in these aggregates influences properties that one would like to take advantage in the design of sensory schemes. A major and yet unanswered challenge rests in determining the exact organization of chains in these aggregates, particularly at low concentrations.

Recent work demonstrated that increasing the counter anion (CA) size can decrease the interchain contacts of copolymer **PFBT-X** (Scheme 1.9), which contains alternating fluorene and BT units, and leads to a substantial increase of quantum yield in the bulk [56]. Size analysis of polymers containing Br^- and $\text{B}[(3,5-(\text{CF}_3)_2\text{C}_6\text{H}_3)]_4^-$ ($\text{BAr}_4^{\text{F}-}$) in water by DLS techniques indicates suppression of aggregation by the large and hydrophobic $\text{BAr}_4^{\text{F}-}$. The



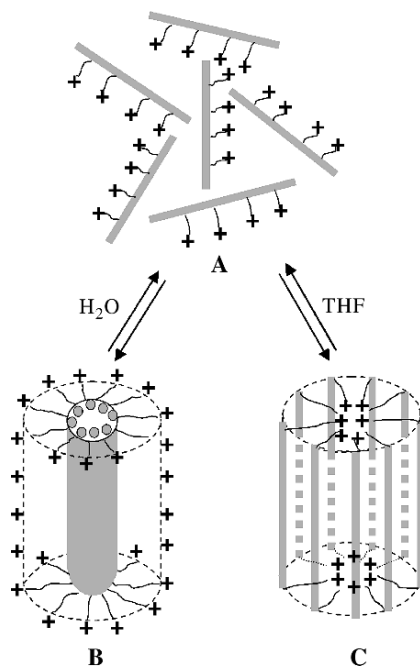
Scheme 1.9. Molecular structure of **PFBT-X**. Reprinted with permission from [56]. Copyright 2006 American Chemical Society

charge compensating ions are, therefore, important structural components in these materials and can be used to regulate optoelectronic properties for specific applications. Starting with a parent structure, simple ion exchange methods can be taken advantage of to generate a range of materials with substantially different performances.

The amphiphilic characteristics of charged poly(fluorene)s lead to different aggregation structures in different solvents as well as optical coupling of the optical partners [57]. In the case of **P1**, there exist two different types of aggregates depending on the solvent medium (Scheme 1.10). Single chain behavior or minor aggregation occurs when the THF content is in the range from 30% to 80% (Scheme 1.10a). These solvent mixtures allow for solvation of both components of the polymer structure. In pure water, the polymer likely forms tight aggregates, with chains coming together and forming the inner core (Scheme 1.10b). Interchain aggregation in water is dominated by hydrophobic interactions, and leads to lower emission intensities due to π - π stacking and self-quenching. Addition of THF to aqueous solutions breaks up the aggregates. Longer interchain distances reduce self-quenching and give rise to higher emission frequencies. When the THF content is higher than 80% the ionic interactions of charged groups with the nonpolar medium lead to the groups becoming buried within a new aggregate structure (Scheme 1.10c), which is dominated by the electrostatic interactions between the charged quaternary amine groups and charge compensating iodide ions [58].

1.3 Signal Transduction Mechanisms in Sensors

Biosensors are devices that transduce a biological recognition event (such as antibody-antigen binding) into measurable signals. A particular function of conjugated polymers is to amplify the signals so that lower concentrations of analyte can be interrogated. Within the context of water-soluble poly(fluorene)s, their action has been primarily to amplify fluorescent signatures. This amplification is the result of a higher optical cross section of



Scheme 1.10. Proposed aggregation modes of **P1** in water with different THF content [58]. Reproduced by permission of The Royal Society of Chemistry

the polymer, relative to small molecule reporters, and efficient FRET to a signaling chromophore that is triggered upon a molecular recognition event.

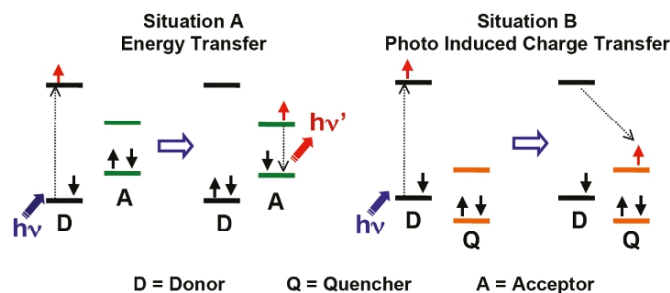
In comparison to intensity-based methods, techniques that rely on FRET provide large changes in emission profiles and open the opportunity for ratiometric fluorescence measurements [59]. Assays of this type are less prone to false positives from nonspecific binding events.

As shown by Förster [60], dipole-dipole interactions lead to long-range resonance energy transfer from a donor chromophore to an acceptor chromophore. Equation (1) describes how the FRET rate changes as a function of the donor-acceptor distance (r), the orientation factor (κ), and the overlap integral (J). The FRET efficiency falls off with the sixth power of distance and thus the modulation of energy-transfer processes provides a ready means for signal generation [59, 60].

$$k_{t(r)} \propto \frac{1}{r^6} \cdot \kappa^2 \cdot J(\lambda) \quad (1.1)$$

$$J(\lambda) = \int_0^\infty k_D(\lambda) \epsilon_A(\lambda) \lambda^4 d\lambda$$

In FRET-based assays, the light harvesting conjugated polymer and a fluorophore capable of introduction into a probe structure are generally designed



Scheme 1.11. Effect of relative orbital energy levels on FRET vs. PCT preferences

to function as the donor and the acceptor, respectively. The overlap integral expresses the spectral overlap between the emission of the donor and the absorption of the acceptor. The components of the sensor can be chosen so that their optical properties meet this requirement.

A competing mechanism to FRET is photo-induced charge transfer (PCT). Although PCT provides the basis for assays that modulate emission intensity, it constitutes an energy-wasting scheme in FRET assays, reducing the intensity of signals and the overall sensitivity. The rate for PCT shows an exponential dependence on the donor–acceptor distance (r), i.e., $k_{PCT} \propto \exp(-\beta/r)$, where β reflects the electronic coupling. Thus, there is a more acute distance dependence relative to (1) and, as we will discuss in the following section, the chemical structure of the polymer chain makes a strong impact on the contribution of the two processes with a given fluorophore reporter.

Scheme 1.11 provides a simplified illustration of two situations that may occur upon excitation of the polymer donor [61]. Situation A corresponds to the ideal situation for FRET, where the HOMO and LUMO energy levels of the acceptor are located within the orbital energy levels of the donor. Upon excitation of the donor, energy transfer to the acceptor takes place, leading to an emissive process, provided that the emission quantum yield of the acceptor is sufficiently large. Similarly, direct excitation of the acceptor under Situation A does not quench the acceptor emission. When the energy levels of the acceptor are not contained within the orbital energies of the donor, in other words when both the electron affinity and the ionization potential are higher in one of the optical partners, as in situation B, donor excitation may lead to PCT [62–66]. As shown in Scheme 1.11, donor excitation would lead to photo-induced electron transfer to the acceptor. Excitation of the acceptor would lead to a similar charge separated state via hole transfer to the donor [61]. Although Scheme 1.11 is widely used for choosing suitable optical partners for a specific application, it fails to be accurate for intermediate cases, since it neglects contributions from the exciton binding energy, the intermolecular charge transfer state energy, and the stabilization of the charged species by the medium. The mechanism by which FRET or PCT is preferred is complex for conjugated polymer blends and may involve geminate electron-hole pairs that

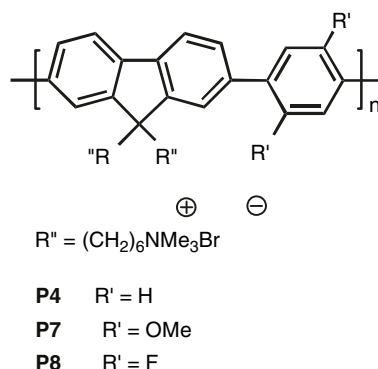
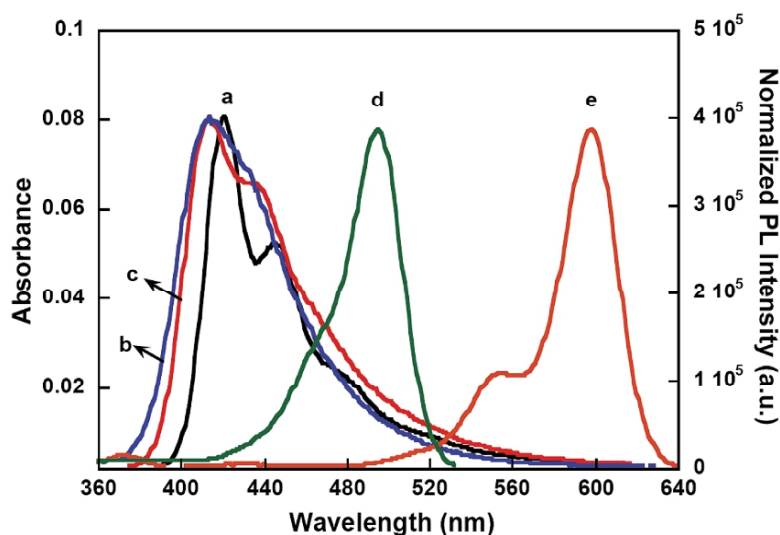
Scheme 1.12. Molecular structures of **P4**, **P7**, and **P8**

Fig. 1.4. Photoluminescence (PL) spectra of **P4** (a), **P7** (b), and **P8** (c) and absorbance of ssDNA-C* (FI, d and TR, e) in 25 mM phosphate buffer (pH 7.4). Excitation wavelength is 385 nm for **P4**, 365 nm for **P7**, and **P8**. Reprinted with permission from [68]. Copyright 2006 American Chemical Society

may convert to exciplexes and ultimately excitons [67]. Despite these uncertainties, Scheme 1.11b provides for a necessary, but not sufficient, condition for PCT.

A series of cationic poly(fluorene-*co*-phenylene) derivatives was prepared to probe the effect of the molecular orbital energy levels on FRET efficiency [68]. As shown in Scheme 1.12, three different polymers were used in which electron donating (OMe, **P7**) or withdrawing (F, **P8**) groups were introduced into the phenylene unit. As shown in Fig. 1.4, the PL spectra of the three polymers

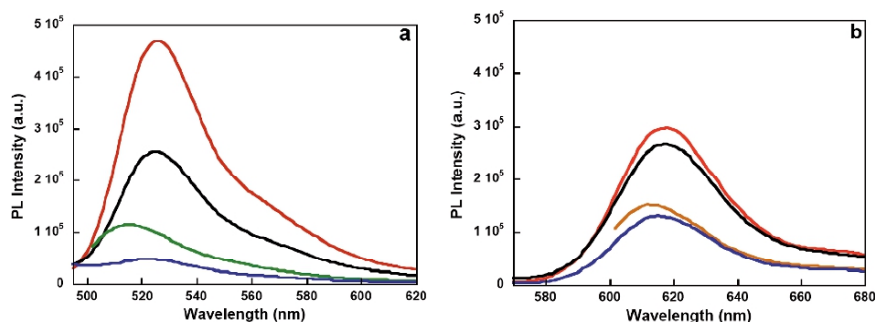


Fig. 1.5. Fluorescence spectra of ssDNA-FI (**a**) and ssDNA-TR (**b**) in the presence of **P4** (*black*), **P7** (*blue*), and **P8** (*red*) in 25 mM phosphate buffer at $[\text{ssDNA} - \text{FI or ssDNA} - \text{TR}] = 2 \times 10^{-8} \text{ M}$ and $[\text{RU}] = 4 \times 10^{-7} \text{ M}$. The excitation wavelengths are 385 nm for **P4** and 365 nm for **P7** and **P8**. Direct excitation of ssDNA-FI and ssDNA-TR *prior* to polymer addition are also shown in *green* and *orange*, respectively. Reprinted with permission from [68]. Copyright 2006 American Chemical Society

are similar; furthermore, they all exhibit nearly identical PL quantum yields. Figure 1.4 also shows the absorbance of two typical dyes used in labeling single-stranded DNA probes (ssDNA) namely, fluorescein (FI) and Texas Red (TR). There is much better spectral overlap between the absorption of FI and the emission of polymers **P4**, **P7**, and **P8**, relative to the situation with TR. By looking at (1), one would estimate nearly identical donor capabilities for the three polymers and that FI would be a better acceptor, relative to TR.

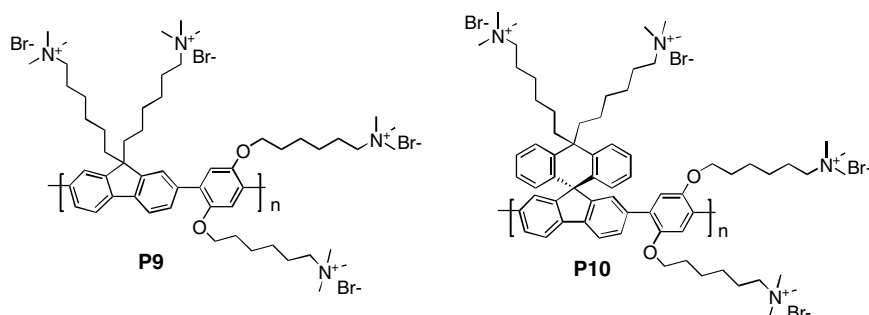
FRET experiments were performed by monitoring dye emission upon excitation of **P4**, **P7**, and **P8** under conditions relevant for biosensor applications and the results are summarized in Fig. 1.5. The most intense FI emission was observed for **P8**/ssDNA-FI, which is approximately twofold more intense than that observed for **P4**/ssDNA-FI and is over an order of magnitude larger than that for **P7**/ssDNA-FI. For **P8**/ssDNA-FI, the integrated FI emission is approximately fivefold greater than that obtained by direct excitation of FI at its absorption maximum (495 nm) in the *absence* of the polymers, while over 20-fold enhancement is observed relative to direct FI excitation in the *presence* of **P8**. This enhancement is indicative of the signal amplification provided by the light harvesting capabilities of the poly(fluorene-*co*-phenylene) backbone. FRET experiments using ssDNA-TR as the acceptor show that TR emission intensities are similar for **P4**/ssDNA-TR and **P8**/ssDNA-TR, which are approximately twice more intense than that observed with **P7**/ssDNA-TR. For **P8**/ssDNA-TR, the integrated TR emission through FRET is approximately twice greater than that obtained by direct excitation of TR at its absorption maximum (590 nm) in the *absence* of the polymers, while there is a tenfold enhancement relative to direct excitation of TR in the *presence* of **P8**. *Of particular significance is that the TR emission*

with **P7**/ssDNA-TR is more intense than the Fl emission with **P7**/ssDNA-Fl, despite the less effective spectral overlap ($J(\lambda)$ in (1)).

Additional experiments with **P4**, **P7**, **P8** ssDNA-Fl and ssDNA-TR revealed the following observations. First, there is self-quenching of the dyes within the conjugated polyelectrolyte/ssDNA-Fl (or ssDNA-TR) aggregates. This effect can be diminished by including unlabeled ssDNA and is less severe for TR than for Fl. Second, there is self-quenching of the polymer emission upon aggregation with unlabeled ssDNA. The exact sizes, shapes, and orientation of the components in these polyplexes are unknown at this stage but are likely to be dominated by the structural attributes of the polyelectrolyte components, namely the rigid backbones and the ssDNA. Third, the three polymers are quenched to the same extent with ssDNA-Fl. In other words, the chemical nature of the dye at the terminus of the ssDNA does not appear to influence the general arrangement of the components so vastly that different optical coupling occurs. Thus, the differences in the sensitization of Fl or TR cannot be attributed to different abilities of **P4**, **P7**, and **P8** to serve as FRET donors.

Examination of the absolute energy levels of the three polymers sheds light into the differences of dye sensitization. Cyclic voltammetry was coupled with optical measurements to estimate the HOMO and LUMO energy levels. Fluorine substitution lowers the energy levels, while the electron donating methoxy group raises the levels, relative to the unsubstituted parent structure **P4**. The Fl LUMO energy is contained within the HOMO-LUMO gap of the three polymers. However, the Fl HOMO energy (-5.9 eV) is lower than those of **P4** (-5.6 eV) and **P7** (-5.4 eV). For these two structures, it is reasonable to expect that situation B in Scheme 1.11, i.e., PCT to the LUMO of Fl, is taking place. For polymer **P8**, with a HOMO energy of -5.8 eV, the situation is less clear and, given the limitations of Scheme 1.11, both processes may be taking place to some extent. The TR HOMO level (-5.4 eV) is higher than those of **P4** and **P8** and is close in energy to the level of **P7**. In fact, the HOMO-LUMO levels of TR are well contained between the levels of **P8**, as in situation A in Scheme 1.11, which favors FRET over PCT. Additionally, the fact that the energy gap difference between TR and the three conjugated polyelectrolytes is smaller than that observed with Fl should provide additional driving force for energy transfer, relative to charge transfer.

Similar comparisons of FRET efficiencies were carried out with poly(9,9'-bis(6-*N,N,N*-trimethylammoniumhexyl)fluorene-*alt*-1,4-(2,5-bis(6-*N,N,N*-trimethylammoniumhexyloxy))phenylene) tetrabromide (**P9**) and poly((10,10'-bis(6-*N,N,N*-trimethylammoniumhexyl)-10H-spiro(anthracene-9,9'-fluorene))-*alt*-1,4-(2,5-bis(6-*N,N,N*-trimethylammoniumhexyloxy))phenylene) tetrabromide (**P10**); structures can be found in Scheme 1.13 [69]. The 10H-spiroanthracenyl group is orthogonal to the main-conjugated backbone vector and was not anticipated to contribute to electron delocalization. These groups behave as "molecular bumpers" that effectively shield the backbone. Accordingly, both **P9** and **P10** show similar absorption and PL spectra and their HOMO and



Scheme 1.13. Molecular structures of **P9** and **P10**

LUMO levels are nearly identical, as determined by electrochemical measurements. The PL quantum yields are also identical within experimental error.

These polymers served as excitation donors to ssDNA-FI. Similar levels of polymer emission quenching are observed upon addition of ssDNA-FI; however, the fate of the excitations is very different. In the case of **P9**, one observes negligible FI emission, whereas for **P10**, it is possible to observe FI emission with a FRET efficiency of 60%. Since the optical properties and orbital energy levels for **P9** and **P10** are identical, the arguments presented for polymers **P4**, **P7**, and **P8** are not applicable to rationalize the differences in optical output. However, it is important to note that FRET and PCT rates, and thereby their probabilities, vary to different extents depending on the donor–acceptor distance. PCT is essentially a contact process described by an exponential distance dependence [61, 70] and functions effectively at D-A distances considerably shorter than those probed by FRET processes (1) [71, 72]. The nearly complete FI emission quenching in **P9**/ssDNA-FI suggests that polymer excitation results in PCT to FI [73]. With **P10**/DNA-FI, one observes much less FI quenching. The introduction of the “molecular bumpers” in **P10** increases the average donor–acceptor distance. This increased separation reduces the probability of PCT, relative to the parent **P9** structure, but allows for FRET to occur with good efficiency. These results indicate that careful attention needs to be paid to molecular design strategies that fine tune distances at the molecular level to favor FRET over quenching by PCT mechanisms.

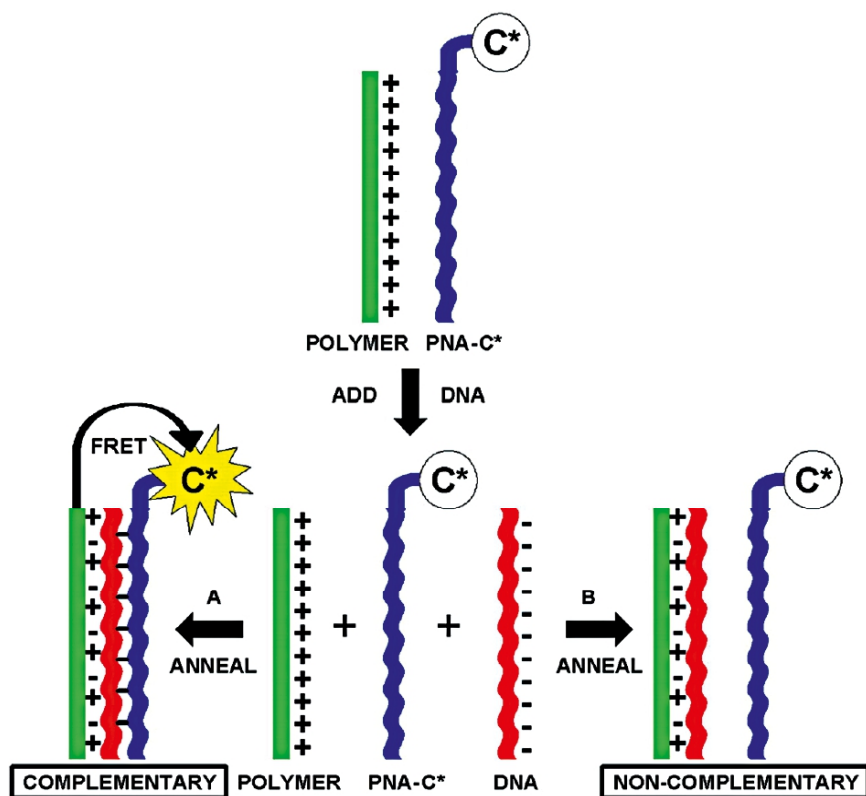
1.4 Chemo- and Biosensor Applications

1.4.1 DNA Sensors

Recent studies using **P2** have shown that it can be used to optically amplify fluorescent DNA assays [74]. The method comprises two components: (a) the light harvesting luminescent conjugated polymer **P2** and (b) a probe oligonucleotide consisting of a peptide nucleic acid (PNA) labeled with a reporter dye

such as F1 (PNA-F1). Addition to the solution of a target polynucleotide with a sequence complementary to the PNA strand yields the duplex structure. Electrostatic interactions bring the conjugated polyelectrolyte in proximity to the PNA/ssDNA-F1 duplex resulting in energy transfer from the polymer to the signaling chromophore. When a nontarget polynucleotide is added, complexation between **P2** and the probe oligonucleotide does not occur. Because the average distance between **P2** and the signaling chromophore is too large for effective energy transfer in the absence of such hybridization, there is little or no emission from the signaling chromophore (Scheme 1.14 and Fig. 1.6). The resulting emission intensity of F1 was enhanced by approximately 25-fold, compared with that obtained upon direct excitation at the absorption maximum of F1.

By adding an S1 nuclease enzyme, it is possible to modify the strategy in Scheme 1.14 so that the overall assay is sensitive to single nucleotide



Scheme 1.14. DNA assay using **P2** (shown in *green*) and PNA-C* (shown in *blue*, where C* is F1). The system responds depending on whether the ssDNA (shown in *red*) is complementary or noncomplementary to the PNA sequence [74]. Copyright 2002 National Academy of Sciences, U.S.A.